PROCEEDINGS OF SCIENCE

Origin of the PeV Photons from the Crab Nebula

Gwenael Giacinti,[a,b,*] **Brian Reville**[c] **and John G. Kirk**[c]

[a] *Tsung-Dao Lee Institute, Shanghai Jiao Tong University, Shanghai 201210, People's Republic of China*

[b] *School of Physics and Astronomy, Shanghai Jiao Tong University, Shanghai 200240, People's Republic of China*

[c] *Max-Planck-Institut für Kernphysik, Postfach 103980, 69029 Heidelberg, Germany*

E-mail: gwenael.giacinti@sjtu.edu.cn, brian.reville@mpi-hd.mpg.de, john.kirk@mpi-hd.mpg.de

Pulsar wind nebulae (PWNe) are known to accelerate electrons to very high energies (VHE), but the acceleration mechanism and site remain uncertain. The pulsar wind termination shock (TS) is a natural candidate for the acceleration site, but the toroidal geometry of the magnetic field there should render shock acceleration inoperative. We propose a solution to this apparent contradiction. We find that drift motion along the shock surface keeps either electrons or positrons in the equatorial region of the TS, where they are accelerated to VHE by the first-order Fermi mechanism. In the present work, we apply our theory to the Crab Nebula, and find that both its high-energy synchrotron emission and its inverse Compton emission can be reproduced by our model. We show that the recent observations by LHAASO of the Crab Nebula up to PeV energies allow for placing new constraints on parameters of the Crab Nebula that are still poorly known. In particular, they provide new insights into the conditions of the striped wind and the immediate downstream of the TS.

38th International Cosmic Ray Conference (ICRC2023)
26 July - 3 August, 2023
Nagoya, Japan

ICRC2023
38th International Cosmic Ray Conference
The Astroparticle Physics Conference

*Speaker

PoS(ICRC2023)839

1. Introduction

The Crab Nebula accelerates electrons to multi-PeV energies [1]. However, their mechanism and site of acceleration remain unclear. X-ray observations of the Nebula [2] are compatible with expectations for electrons accelerated by the first order Fermi mechanism at an ultra-relativistic shock [3, 4]. However, the magnetic field is expected to be toroidal close to the pulsar wind termination shock (TS), which should render particle acceleration inefficient [5, 6]. This field should change sign across the equatorial plane of the pulsar [7]. As demonstrated in [8–10], diffusive shock acceleration should still operate in this region. We calculate here the resulting emission in X-rays and gamma-rays from the Crab Nebula, in our model [8].

2. Model

In the following, we use the model presented in Ref. [8], where electron and positron acceleration takes place in the equatorial region of the TS. We refer the reader to [8] for more details about our simulations. In Fig. 1 we provide a sketch of this region of interest in the Crab Nebula.

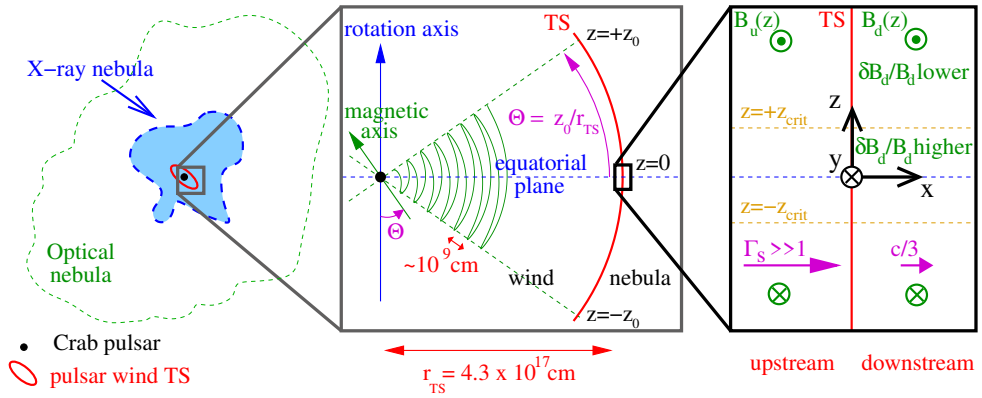

Figure 1: Sketch of the Crab Nebula (left panel), with the location and characteristics of the region studied in this work (right panel).

In the left panel of Fig. 1, the X-ray and optical nebulae are drawn as they appear on the sky, together with an estimate of the position of the TS. The centre panel is an enlargement of the equatorial region of the Crab pulsar wind (labelled "wind"). The TS is drawn as a solid red arc of radius $r_{\rm TS} \simeq 4.3 \times 10^{17}$ cm. The rotation axis of the pulsar (blue arrow) lies in the plane of the figure, and the magnetic axis (green arrow) is drawn at a phase at which it lies in this plane too. The horizontal dashed blue line corresponds to the equatorial plane. Magnetic field oscillations, or stripes, are present upstream of the TS between the latitudes $\pm\Theta$, where Θ is the angle between the magnetic and rotation axes. Upstream, the magnetic field is toroidal and changes sign across the current sheet (thin green line). The stripes are destroyed at (or before) the TS, leaving a net toroidal component in the downstream "nebula", which reverses across the equatorial plane, and has an amplitude that grows with distance from this plane [7]. The black rectangle in the centre panel, and its enlargement in the right panel correspond to the region we model. It is typically a few percent of the shock area, so we take the TS to be plane and the flow planar. In the cartesian

coordinate system defined in Fig. 1, the fluid flows along $+\hat{\mathbf{x}}$. In the simulations, we set the Lorentz factor of the fluid in the upstream ($x < 0$) to $\Gamma_s = 100$. Downstream, the fluid velocity is assumed to be $c/3$, and the residual toroidal field, defined in the downstream rest frame (DF), is labelled as $\mathbf{B}_d(z)$ — with $z_0 = \Theta\, r_{TS}$ and $B_{d,0} = B_d(z_0) = +1$mG. On top of the toroidal field, we add in the downstream a homogeneous 3D turbulent magnetic field, with RMS strength δB_d (defined in the downstream rest frame). The turbulent field is defined on nested 3D grids, repeated periodically in space, using the method of [11]. We use isotropic turbulence with a Bohm spectrum, and with an outer scale equal to $L_{max} = 10^{18}$ cm $\approx 2\, r_{TS}$ unless specified otherwise. We inject electrons and positrons at the TS with their momenta directed along $+\hat{\mathbf{x}}$, and with an energy $E_{inj,d} = 1$ TeV. We integrate the particle trajectories in the shock region, and take synchrotron losses into account.

3. Results

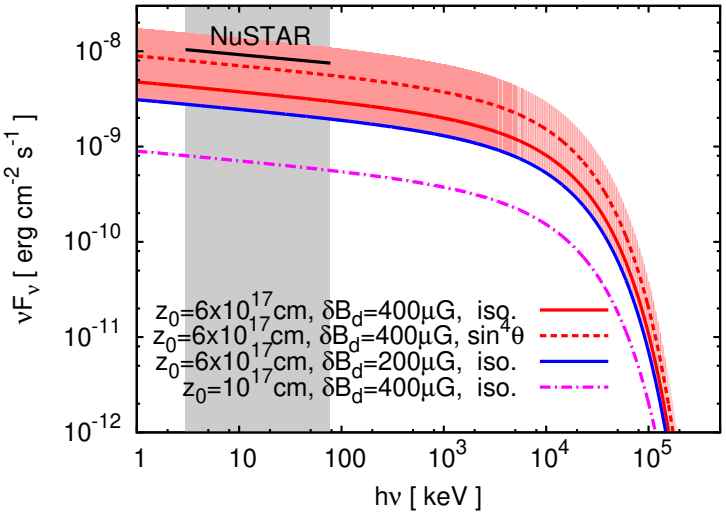

Figure 2: Predicted synchrotron spectra for the Crab Nebula versus NuSTAR measurements.

We calculate, from our numerical simulations, the synchrotron spectrum from cooled electrons in the Nebula. We plot our results in Fig. 2, for four sets of parameter values. See the key for the values of z_0 and δB_d, and for the isotropy ("iso.") or anisotropy of the pulsar wind. We consider both isotropic and $\propto \sin^4\theta$ winds, where θ denotes the colatitude. We use 2.0 kpc for the distance to the Crab pulsar. The effect of the uncertainty on this distance (±0.5 kpc) for the two red lines is shown with the area shaded in red. The solid black line corresponds to the measurements from NuSTAR in the 3 − 78 keV band [2]. Our model can reproduce them for sufficiently large values of δB_d ($\geq 200\,\mu$G) and z_0. The magenta dashed-dotted line for $z_0 = 10^{17}$ cm (i.e., $\Theta \simeq 13°$) and $\delta B_d = 400\,\mu$G is about an order magnitude below the measurements, but we obtain a larger X-ray flux for $z_0 = 6{\times}10^{17}$ cm (i.e., $\Theta \simeq 80°$): the blue and red solid lines correspond to $\delta B_d = 200\,\mu$G and $\delta B_d = 400\,\mu$G for an isotropic wind. The red dashed line is for a $\propto \sin^4\theta$ wind and $\delta B_d = 400\,\mu$G. We can reproduce the data with these parameters. $|\mathbf{B}_d|(z) \propto |z|$ here, and the measurements would be reproduced with smaller values of Θ and δB_d, if one adopts a shallower dependence of $|\mathbf{B}_d|$ on

z, such as in the profile in Komissarov's 2013 model [12]. With this profile, we find that we can reproduce the data well with $\Theta = 60^\circ$ and $\delta B_{\rm d} = 100\,\mu$G only.

In Figs. 3 and 4, we present our calculations of the gamma-ray spectrum of the Crab Nebula with this "Komissarov profile", and with a $\propto \sin^4\theta$ wind. We also assume here that $\delta B_{\rm d} = 100\,\mu$G and $\Theta = 60^\circ$. For the background photon fields, we use the values from the "constant B-field model" with $B = 125\,\mu$G of Ref. [13], and the distributions of the electron and photon densities in the Nebula that are provided in this same reference. We plot the LHAASO data points from Ref. [14].

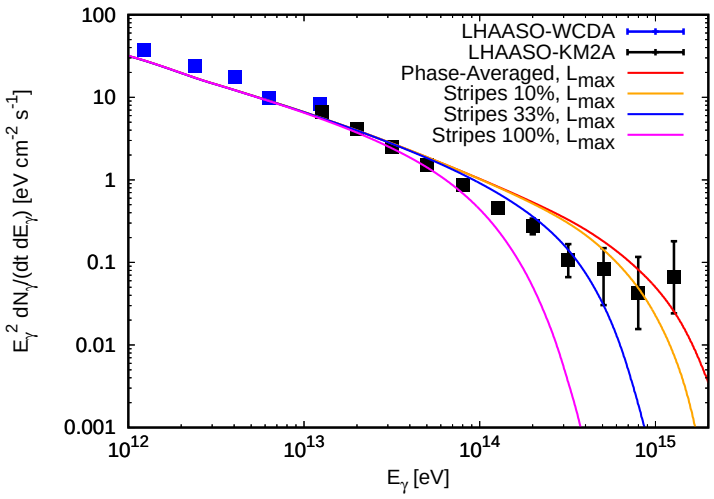

Figure 3: Gamma-ray spectrum of the Crab Nebula in our model, for $\Theta = 60^\circ$, $\delta B_{\rm d} = 100\,\mu$G, a $\propto \sin^4\theta$ wind, and a "Komissarov profile" [12] for $|\mathbf{B}_{\rm d}|$. The red line is for our reference case with an outer scale $L_{\rm max} = 10^{18}\,{\rm cm} \approx 2\,r_{\rm TS}$ and where electrons cool in the phase-averaged field in the upstream. The orange blue and magenta lines are for the case where the stripes survive up to the TS, and where electrons cool in 10%, 33%, and 100% of the full amplitude of the upstream magnetic field. The LHAASO data points are taken from Ref. [14].

The red curve in both figures shows the results for our reference case with an outer scale $L_{\rm max} = 10^{18}\,{\rm cm} \approx 2\,r_{\rm TS}$, and where electrons cool in the phase-averaged field in the upstream. This curve fits well the existing observations of the Crab Nebula at energies $\lesssim 200\,$TeV, and predicts that, for these parameters, the spectrum would continue unabated up to $\sim$ PeV energies, and almost look like a pure power-law. Our predictions for the shape of the high-energy end ($\gtrsim 200\,$TeV) of the gamma-ray spectrum depends on unknown parameters of the Crab wind and Nebula.

In Fig. 3, we show the dependence of the spectrum on the upstream magnetic field parameters. The magenta line shows the case where the stripes are assumed to survive up to the TS, and where the electrons cool in the full amplitude of the upstream magnetic field (assuming that $B_{\rm d,0} = 1\,$mG). In this case, the emission has a sharp turnover at lower energies, and the emission is strongly suppressed above $\approx 200\,$TeV. This is due to the fact that synchrotron cooling is more important when the stripes survive up to the TS and the magnetic field is therefore stronger close to the TS. The blue and orange lines show intermediate cases where the stripes partially survive up to the TS, but where the amplitude of the field in which the electrons cool in the upstream is only $1/3$ and

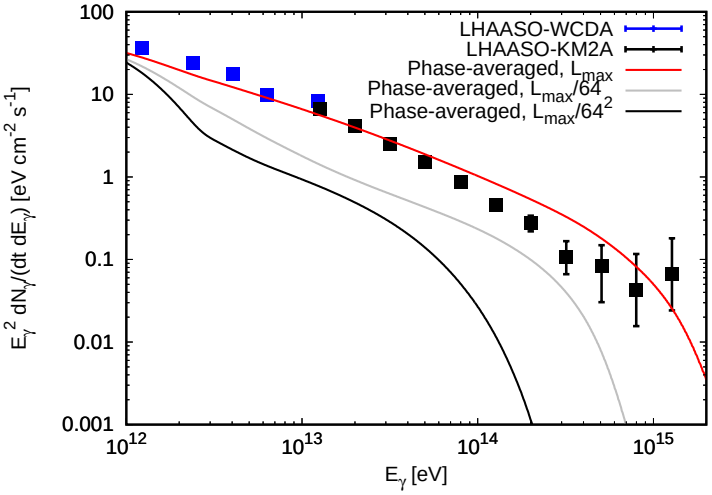

Figure 4: Same as in Fig. 3. The grey and black lines are for outer scales equal to $L_{\rm max}/64$ and $L_{\rm max}/64^2$. The LHAASO data points are taken from Ref. [14].

$1/10$ of the full amplitude of this field.

In Fig. 4, we show how results depend on the value of the outer scale of the turbulence, by reducing it. In this panel, we assume that the upstream magnetic field is the phase-averaged one for all 3 curves. The grey curve shows our calculations for an outer scale equal to $L_{\rm max}/64$ (where $L_{\rm max} = 10^{18}$ cm) and the black curve is for an outer scale equal to $L_{\rm max}/64^2$. One can clearly see that the maximum photon energy diminishes for decreasing values of the outer scale. This is due to the fact that very-high energy electrons are not strongly scattered by the turbulence any more once their gyroradius exceeds the outer scale of the turbulence. This shuts down the acceleration process at high energies. The fact that the gamma-ray fluxes are lower for the grey and black curves at $\sim 1-10$ TeV is due to the fact that some of the electrons injected in the favourable equatorial region already have a gyroradius that is larger than the outer scale of the turbulence, which prevents them from being scattered into the upstream and accelerated.

4. Conclusions

We studied here particle acceleration at the TS of a striped pulsar wind. We find that the acceleration of X-ray emitting electrons occurs preferentially in the equatorial region of the TS. Our model can reproduce well the observed X-ray and TeV–PeV gamma-ray spectra of the Crab Nebula. We show that the shape of our predicted gamma-ray spectra at the high-energy end ($\gtrsim 100$ TeV) depends on unknown parameters of the Crab pulsar wind and Nebula. Comparing our predictions with the published LHAASO data [14] allows to disentangle between different scenarios for the upstream magnetic field and downstream turbulence, and to place new constraints on unknown parameters of the Crab pulsar wind and Nebula.

References

[1] R. Bühler, R. Blandford, *The surprising Crab pulsar and its nebula: a review*, *Rep. Prog. Phys.* **77** (2014) 066901 [arXiv:1309.7046].

[2] K. Madsen *et al.*, *Broadband X-ray Imaging and Spectroscopy of the Crab Nebula and Pulsar with NuSTAR*, *ApJ* **801** (2015) 66 [arXiv:1502.07765].

[3] J. Bednarz, M. Ostrowski, *Energy Spectra of Cosmic Rays Accelerated at Ultrarelativistic Shock Waves*, *Phys. Rev. Lett.* **80** (1998) 3911 [astro-ph/9806181].

[4] J. G. Kirk, A. W Guthmann, Y. A. Gallant, A. Achterberg, *Particle Acceleration at Ultrarelativistic Shocks: An Eigenfunction Method*, *ApJ* **542** (2000) 235 [astro-ph/0005222].

[5] M. C. Begelman, J. G. Kirk, *Shock-Drift Particle Acceleration in Superluminal Shocks: A Model for Hot Spots in Extragalactic Radio Sources*, *ApJ* **353** (1990) 66.

[6] L. Sironi, A. Spitkovsky, *Particle Acceleration in Relativistic Magnetized Collisionless Pair Shocks: Dependence of Shock Acceleration on Magnetic Obliquity*, *ApJ* **698** (2009) 1523 [arXiv:0901.2578].

[7] O. Porth, M. J. Vorster, M. Lyutikov, N. E. Engelbrecht, *Diffusion in pulsar wind nebulae: an investigation using magnetohydrodynamic and particle transport models*, *MNRAS* **460** (2016) 4135 [arXiv:1604.03352].

[8] G. Giacinti, J. G Kirk, *Acceleration of X-Ray Emitting Electrons in the Crab Nebula*, *ApJ* **863** (2018) 18 [arXiv:1804.05056].

[9] B. Cerutti, G. Giacinti, *A global model of particle acceleration at pulsar wind termination shocks*, *Astron. Astrophys.* **642** (2020) A123 [arXiv:2008.07253].

[10] B. Cerutti, G. Giacinti, *Formation of giant plasmoids at the pulsar wind termination shock: A possible origin of the inner-ring knots in the Crab Nebula*, *Astron. Astrophys.* **656** (2021) A91 [arXiv:2111.04337].

[11] G. Giacinti, M. Kachelriess, D. V. Semikoz, G. Sigl, *Cosmic ray anisotropy as signature for the transition from galactic to extragalactic cosmic rays*, *JCAP* **7** (2012) 031 [arXiv:1112.5599].

[12] S. Komissarov, *Magnetic dissipation in the Crab nebula*, *MNRAS* **428** (2013) 2459 [arXiv:1207.3192].

[13] M. Meyer, D. Horns, H.-S. Zechlin, *The Crab Nebula as a standard candle in very high-energy astrophysics*, *Astron. Astrophys.* **523** (2010) A2 [arXiv:1008.4524].

[14] Z. Cao *et al.* [LHAASO Collaboration], *Peta-electron volt gamma-ray emission from the Crab Nebula*, *Science* **373** (2021) 425.